Preliminary measurements of the edge magnetic field pitch from 2-D Doppler backscattering in MAST and NSTX-U (invited)

R. G. L. Vann, K. J. Brunner, R. Ellis, G. Taylor, and D. A. Thomas

---

Articles you may be interested in

Process to generate a synthetic diagnostic for microwave imaging reflectometry with the full-wave code FWR2Da)
Rev. Sci. Instrum. **85**, 11D863 (2014); 10.1063/1.4895100

High-resolution tangential absolute extreme ultraviolet arrays for radiated power density measurements on NSTX-Ua)
Rev. Sci. Instrum. **85**, 11D859 (2014); 10.1063/1.4894835

2D microwave imaging reflectometer electronicsa)
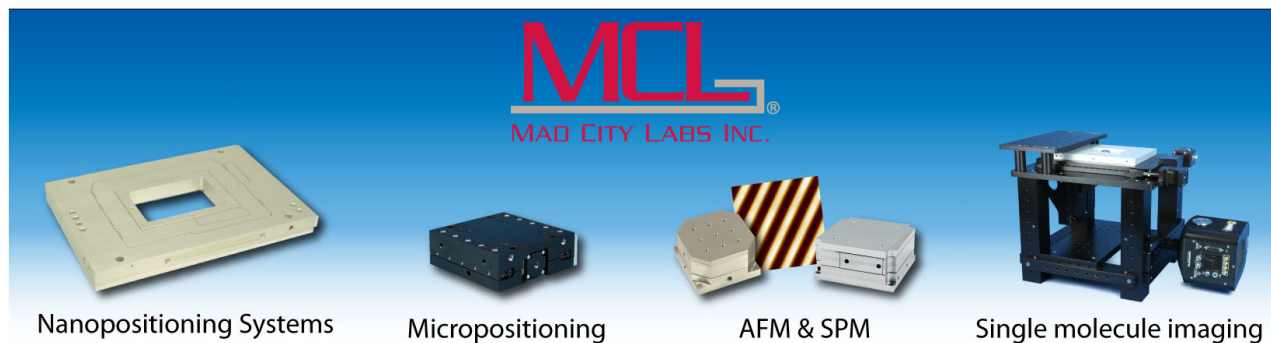Rev. Sci. Instrum. **85**, 11D834 (2014); 10.1063/1.4891047

Technical overview of the millimeter-wave imaging reflectometer on the DIII-D tokamak (invited)a)
Rev. Sci. Instrum. **85**, 11D702 (2014); 10.1063/1.4889735

Simultaneous microwave imaging system for density and temperature fluctuation measurements on TEXTOR (invited)
Rev. Sci. Instrum. **75**, 3787 (2004); 10.1063/1.1794864

Preliminary measurements of the edge magnetic field pitch from 2-D Doppler backscattering in MAST and NSTX-U (invited)

R. G. L. Vann,[1,a)] K. J. Brunner,[2] R. Ellis,[3] G. Taylor,[3] and D. A. Thomas[1,4]

[1]*York Plasma Institute, Department of Physics, University of York, York YO10 5DD, United Kingdom*
[2]*Centre for Advanced Instrumentation, Department of Physics, Durham University, Durham DH1 3LE, United Kingdom*
[3]*Princeton Plasma Physics Laboratory, Princeton, New Jersey 08543, USA*
[4]*Culham Centre for Fusion Energy, Culham Science Centre, Abingdon OX14 3DB, United Kingdom*

The Synthetic Aperture Microwave Imaging (SAMI) system is a novel diagnostic consisting of an array of 8 independently phased antennas. At any one time, SAMI operates at one of the 16 frequencies in the range 10-34.5 GHz. The imaging beam is steered in software post-shot to create a picture of the entire emission surface. In SAMI's active probing mode of operation, the plasma edge is illuminated with a monochromatic source and SAMI reconstructs an image of the Doppler back-scattered (DBS) signal. By assuming that density fluctuations are extended along magnetic field lines, and knowing that the strongest back-scattered signals are directed perpendicular to the density fluctuations, SAMI's 2-D DBS imaging capability can be used to measure the pitch of the edge magnetic field. In this paper, we present preliminary pitch angle measurements obtained by SAMI on the Mega Amp Spherical Tokamak (MAST) at Culham Centre for Fusion Energy and on the National Spherical Torus Experiment Upgrade at Princeton Plasma Physics Laboratory. The results demonstrate encouraging agreement between SAMI and other independent measurements. *© 2016 Author(s). All article content, except where otherwise noted, is licensed under a Creative Commons Attribution (CC BY) license (http://creativecommons.org/licenses/by/4.0/).* [http://dx.doi.org/10.1063/1.4962253]

I. MOTIVATION

The stability and performance of tokamaks operating in the so-called high confinement mode ("H-mode") depends strongly on the transport barrier that develops in the plasma edge. The very narrowness of this layer (typically only ~2% of the minor radius) makes it difficult to characterise. An issue associated with H-mode operation is the appearance of edge localised modes[1] (ELMs). The role of ELMs in flushing the plasma of impurities may be beneficial, but this is at the cost of potentially damaging localised heat loading on plasma facing components. The heat loading generated by ELMs on next generation devices such as ITER necessitates these instabilities either be eliminated entirely or else that their frequency be increased so that the energy released during each ELM is sufficiently reduced.

A simplified representation of the ELM cycle is shown in Figure 1 illustrating the ELM cycle as a path through a configuration space characterised by edge pressure gradient and edge current density. Immediately following an ELM, the plasma is stable and resides in the green shaded region. As the plasma heats up, the edge pressure gradient increases. This may then lead to an increase in the edge current density via, for example, the bootstrap mechanism. Departure from the green region leads to instability and the triggering of an ELM crash — either due to excess pressure gradient (exciting a "ballooning" mode) or excess current density (exciting a "peeling" mode). The distance in configuration space travelled during the crash is related to the stored energy that is released; relatively small cycles (indicated by the orange and purple arrows) may be sufficiently small as to be unproblematic. However, a large crash (indicated by the blue arrows) may lead to damage of plasma-facing components. In order to develop and constrain meaningful models of ELMs, observations of ELMs from experiments are used to locate points on the stability boundary; these observations are then compared with model calculations of the stability boundary. Being able to locate an ELM event on the stability diagram depends on good diagnostics. The edge pressure gradient can be measured using Thomson scattering.[2,3] However, measuring the edge current density with high resolution in both time and space has proved to be more challenging — the vertical coordinate on the stability diagram is typically calculated from models, e.g., by using a neoclassical model to calculate the bootstrap current from the edge pressure gradient. This reliance on a model is unsatisfactory since the model may not capture all the relevant physics. There is consequently a significant effort at the present time to develop diagnostics that can make routine measurements of the edge current density with sufficient spatial and temporal resolution for input into edge stability models. Various techniques presented at this conference include measurement of motional Stark effect (MSE),[4] beam emission polarimetry,[5] and reverse imaging of O-X mode conversion windows.[6]
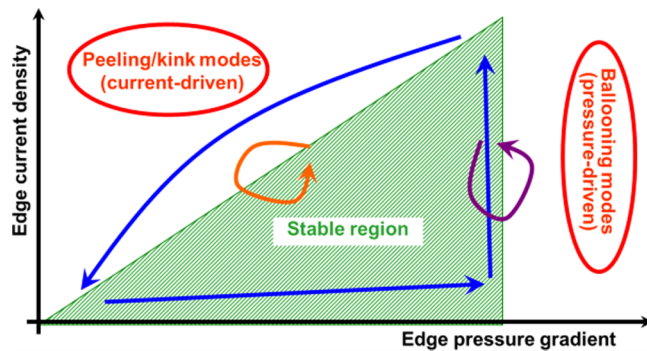
FIG. 1. Simplified diagram of the ELM cycle; small ELMs (represented by the purple and orange arrows) may be operationally acceptable; a large ELM (represented by the blue arrows) may be damaging to plasma facing components. Comparing experimentally observed instability thresholds to those predicted by theory is crucial for understanding the physics of ELMs; the problem being addressed by SAMI is that no method currently exists for the routine measurement of the edge current density.

Synthetic Aperture Microwave Imaging's (SAMI) ultimate objective is similarly to make measurements of the magnetic pitch angle and thence the edge current density, but with better spatial and temporal resolution than other diagnostics.

II. PRINCIPLES OF PHASED-ARRAY IMAGING

Phased-array imaging is an interferometric technique: it uses the phase of the signal at each antenna, rather than focusing optics, to determine the emission pattern. Specifically, we steer the imaging beam by adjusting the phase at each antenna so that constructive interference between the beams from all antennas in the array occurs in the direction of interest. Unlike a directly focused system, the resolution is proportional to the square of the number of antennas (since it depends on the number of cross-correlations that can be made between antenna pairs) at the cost of having to capture the phase, as well as the amplitude, of the signal at each antenna.

Aperture synthesis was pioneered as a technique in radio astronomy[7,8] and is now used widely in that field (see Ref. 9 for a comprehensive review). However, to the best of our knowledge, SAMI is the first diagnostic to employ 2-D phased-array imaging in a laboratory plasma diagnostic.

III. 2-D DOPPLER BACK-SCATTERING (DBS)

The theory of Doppler back-scattering (DBS) is not entirely straightforward; a review of conventional DBS may be found in Ref. 10 and a detailed description of the extension to 2-D is given in Ref. 11. The technique for measuring magnetic pitch angle relies on the cut-off surface being corrugated, for example, as a consequence of turbulence. These corrugations are assumed to be elongated along field lines, since parallel transport is much faster than perpendicular transport. When the plasma is illuminated, the strongest reflected signal comes from the region on the plasma surface normal to the beam. However, this component has only a small Doppler shift and so, assuming the plasma is rotating poloidally and/or toroidally, can be filtered out. The strongest Doppler-shifted

signal comes from the regions of the plasma where the density corrugations (and hence magnetic field lines) are perpendicular to the line of sight. The line segment joining the points of strongest blue- and red-shift is therefore expected to be perpendicular to the magnetic field.

In practice, we construct our 2-D Doppler map post-shot by scanning across the field of view at $161 \times 161 = 25\,921$ locations using "beam steering": we apply the relative phase at each antenna required to achieve constructive interference at each location; the phase-shifted time series are added and the sum is frequency-filtered in order to extract the red- and blue-shifted powers in the range 10-200 kHz either side of the probing frequency. As shown in Fig. 2, we then construct a map showing the difference between the red and blue shifted power. The maximum and minimum in this power difference are interpreted as the locations of maximum Doppler shift away from and towards the array. Our measurement of the pitch angle is the direction perpendicular to the line segment joining these two extrema. A more detailed description of this method is given in Ref. 11.

SAMI is a proof-of-principle device and is equipped with only 8 antennas. Consequently the dominant source of error is the width of the main beam (FWHM $\pm 10°$ at 15 GHz) and the side-lobe level (-7 dB). To enable SAMI to become a production diagnostic rather than a proof-of-principle device, more antennas are required to reduce the width of the main beam and decrease the side-lobe level. Additional sources of error exist, including cross-talk between antennas, wave polarisation effects, and near-field image inversion effects. However, these factors will affect the measurement much less than having only a limited number of antennas. A first estimate of the error might be the main beam width, but it is conceivable that this is an over-estimate; for example, a phased array can locate a point source with an accuracy much better than the width of its main beam. Making a quantitative estimate of the error is challenging without full-wave modelling of the system, which is currently underway using the EMIT-3D code.

Although not attempted in this paper, by measuring the field line pitch at more than one frequency (and therefore more than one location, localised by Thomson scattering), using the
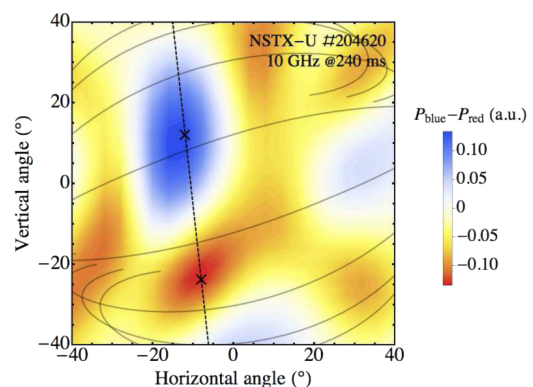

FIG. 2. SAMI measurement of power imbalance between red and blue Doppler-shifted components of the back-scattered microwave radiation for NSTX-U shot 204620 shown as a function of horizontal and vertical viewing angles. The dashed line, which we expect to be perpendicular to the magnetic field, joins the extrema in Doppler shift imbalance; the solid lines show the magnetic field calculated by EFIT.
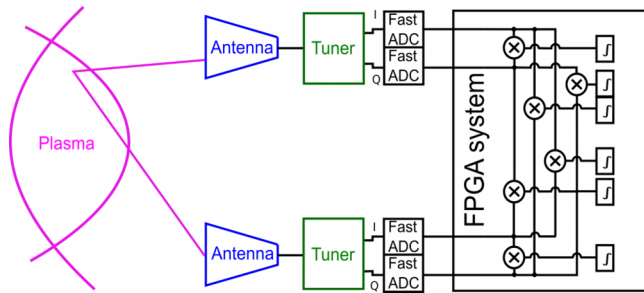
FIG. 3. Simplified diagram of the SAMI hardware. Each of the three sections (i) antenna array (shown in blue), (ii) microwave tuner (shown in green), and (iii) FPGA-based digitisation system (shown in black) are described in the text.

$1/R$ dependence of the toroidal field in the plasma edge to derive the total field and then applying Ampère's Law, we can in principle use SAMI to calculate the edge current density.

IV. HARDWARE DESCRIPTION

In this section, we provide an overview of the SAMI hardware; a more detailed description is provided in Ref. 12. A simplified diagram of the SAMI hardware is shown in Figure 3. We decided to perform the cross-correlations in software rather than by using mixers. This is beneficial because (i) it permits greater flexibility and control (particularly in terms of calibration) and (ii) the number of mixers scales like the square of the number of antennas, but it comes at the cost of more demanding digitisation.

SAMI has 16 independent frequency channels in the range 10-34.5 GHz. This frequency range is chosen to cover the steep gradient region in the edge of H-mode plasmas. The cutoffs for O-mode and X-mode for the National Spherical Torus Experiment Upgrade (NSTX-U) plasmas operating in both L-mode and H-modes are shown for two different times during shot 204672 in Figure 4. The distance between the cut-off surfaces corresponding to the neighbouring SAMI frequency channels in the steep gradient region in H-mode is typically <1 mm; this increases for L-mode and outside the steep gradient region. This tight spacing of cut-off surfaces means that, at least in the steep gradient region in H-mode, SAMI has excellent spatial resolution.

A. Antenna array

The SAMI antenna array consists of 10 Vivaldi PCB antennas, each measuring 20×60 mm. These antennas provide good broadband response in the desired range 10-34.5 GHz, a wide field of view (in excess of $\pm 40°$ in both E and H planes) and excellent polarisation separation perpendicular and parallel to the plane in which the PCBs are oriented. Additionally they are very cheap to manufacture. However, they have the disadvantage that the array is 3-D and so the incoming signal is reflected around inside the array. Eight of the antennas are used as a receiving array; their placement has been chosen to maximise the mean beam efficiency (i.e., to minimise the side-lobe power).[13] The remaining two antennas are used to launch a broad illuminating beam at a user-determined frequency (typically 12.5 MHz) above the probing frequency.
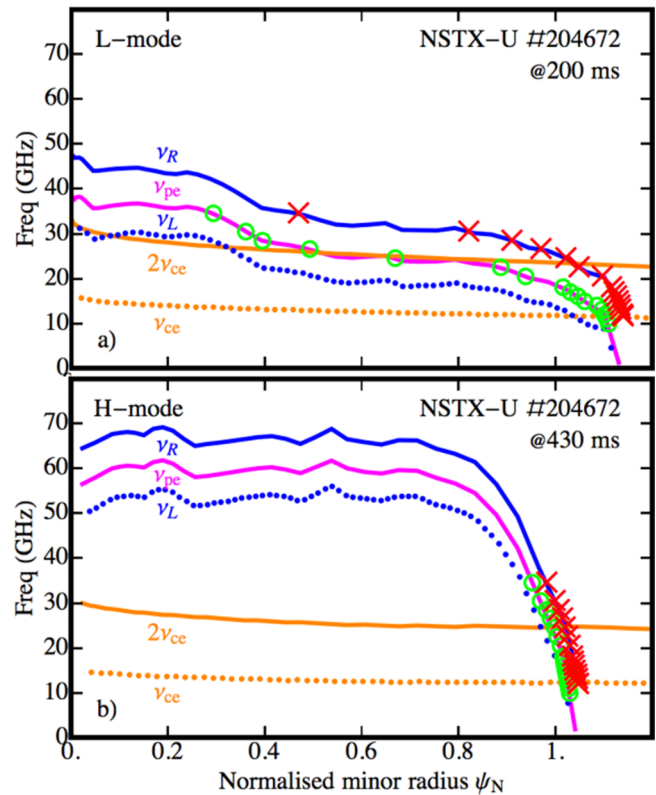

FIG. 4. Diagram showing the electron cyclotron frequency (dashed orange) and its second harmonic (solid orange), the left-hand (dashed blue) and right-hand (solid blue) cutoffs, and the plasma frequency (magenta). The O-mode and X-mode cut-off locations for each of SAMI's 16 frequency channels are shown as green circles and red crosses, respectively. Plots are shown for NSTX-U shot 204672 at two different times, namely, (a) 200 ms and (b) 430 ms into the shot, demonstrating how the distribution of SAMI cut-off locations in the plasma changes from L-mode to H-mode. The cut-off spacing between frequency channels in H-mode is typically <1 mm.

The back-scattered signal has a bandwidth of 3 MHz and consequently SAMI can image both the spontaneous thermal plasma emission and the back-scattered signal simultaneously by frequency-separating the relevant parts of the spectrum.

All the antennas in the array measure the same plane of polarisation of the incoming radiation. Since the edge pitch angle varies substantially, there has been no attempt to orient the antennas in a particular way with respect to the magnetic field. The antennas therefore receive a mixture of O-mode and X-mode signals which we are unable to separate. Not only does this mixing of polarisations reduce the signal-to-noise ratio, but it also enables interference to occur between the signals reflected from the O and X-mode cutoffs. An accurate estimate of the resulting error can be calculated using a full-wave code; this work is currently underway. However, it is likely that in the steep gradient region, where the cutoffs are close together, interference between cut-off layers will increase the fluctuation level of the result but have only a small effect on its time average.

B. Microwave tuner

The microwave tuner unit operates using the standard heterodyne down-conversion principle. The signal from each

receiving antenna is amplified by a low-noise amplifier, split into in-phase and quadrature (I and Q) components by a 90° phase-shifter, and frequency down-converted using second harmonic mixers. A reverse process generates the active probing signal on the two transmitting antennas. Connectorised components are used throughout to simplify assembly and reduce design overhead. There are 16 local oscillator sources of dielectric resonance oscillator type approximately evenly spaced (avoiding exact harmonics) in the range 5-17.25 GHz; the choice of source can be switched with a settling time of 100 ns.

C. FPGA-based digitisation system

The digitisation requirements are demanding: SAMI acquires data at 250×10^6 samples/s and 14 bits/sample (2 aligned bytes), corresponding to a total data rate of 8 GB/s continuously over a shot length of 500 ms. We designed and built a custom data acquisition unit based on 4DSP's FMC108 ADC card and Xilinx's ML605 FPGA board running embedded Linux.[14] A number of enhancements have been made for SAMI's move from Mega Amp Spherical Tokamak (MAST) to NSTX-U as described in Ref. [15]. The standard aperture synthesis image inversion is performed using a CUDA code on an nVidia GPU card[16] which provides at least an order of magnitude speed-up relative to calculation on a standard CPU. An advantage of phased-array imaging is that, in order to overcome near-field effects, the focal length of the imaging beam can adjusted in software post-shot (and as a function of viewing direction, if so desired).

V. DEPLOYMENT ON MAST AND NSTX-U

SAMI was originally deployed on the Mega Amp Spherical Tokamak[17] (MAST) at Culham Centre for Fusion Energy for the period 2011-2013. During this time, SAMI successfully demonstrated the feasibility of 2-D phased-array microwave imaging. In "passive imaging" mode, it captured the first 2-D images of O-X-B mode conversion from a tokamak plasma[18] and demonstrated the existence of strong microwave bursts during ELMs (explained via the anomalous Doppler instability).[19] In "active probing" mode, it made the first measurements of edge pitch angle using 2-D Doppler back-scattering,[11] some results from which are presented in this paper for the first time.

Following the commencement of construction of MAST-Upgrade, SAMI was moved to Princeton Plasma Physics Laboratory where it was installed on the National Spherical Torus Experiment Upgrade[20] (NSTX-U) with only minor modifications to the hardware. SAMI began collecting data on May 3, 2016. The first data from SAMI on NSTX-U are presented in this paper.

As shown in Figure 5, the SAMI antenna array is installed on NSTX-U at the outboard midplane. SAMI has a good view of the plasma (extent shown in green in the figure). The nearest point on the plasma last closed flux surface (LCFS) (ray shown in red in the figure) is approximately 0.5 m from the array. We have illustrated the critical density flux surfaces corresponding to each of SAMI's frequency channels by
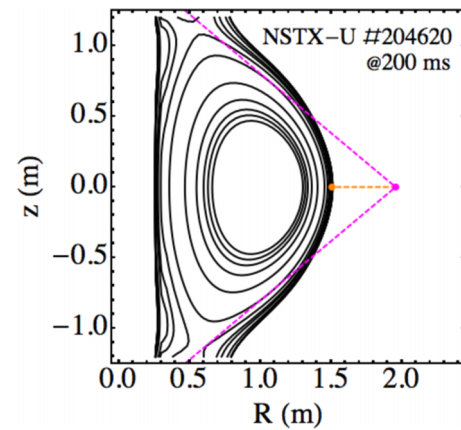

FIG. 5. Diagram showing installation position of the SAMI antenna array on NSTX-U and the critical density flux surfaces for SAMI's frequency channels for NSTX-U shot 204620 at 200 ms (derived from the midplane Thomson scattering data and approximating density to be a flux function). SAMI's field of view is shown in magenta; the normal viewing ray is shown in orange.

using the midplane Thomson scattering data and approximating density to be a flux function. On MAST, SAMI was located approximately 1 m away from the plasma LCFS and 20 cm above the midplane; the view was partially obscured by one of the poloidal field coils. The location on NSTX-U is an improvement since there are no vessel components obscuring the view, the proximity to the plasma increases the amplitude of the back-scattered signal (see below), and the location on the midplane will enable future studies testing theories of polarisation-dependent asymmetries in OXB mode conversion in double null discharges. However, the distance between the antennas and the plasma is now only approximately three times the largest distance between antenna pairs, which means that we are approaching the near field. This may necessitate some further development of our image inversion algorithms.

VI. RESULTS

Typical Doppler-shifted spectra from an individual SAMI antenna from both MAST and NSTX-U are shown in Figure 6. The spectra shown in magenta are measured before the start of the shot, i.e., when no plasma is present. As expected, the reflected signal has relatively narrow bandwidth (since the surfaces from which the beam is reflecting are stationary). The spectra shown in blue are measured during a shot, i.e., when plasma is present. As expected, there is a significant increase in the Doppler-shifted power. Moreover, we observe that the Doppler-shifted power on NSTX-U is significantly greater than the Doppler-shifted power on MAST due to the antenna array being closer to the plasma surface on NSTX-U. Unlike conventional "single ray" Doppler back-scattering, the signal comes not from a small region of the plasma but from an extended area. Consequently the Doppler spectrum that SAMI sees is not a well-defined spike (at a frequency proportional to the plasma velocity) but rather a smeared-out spectrum. Steering the beam using all eight antennas leads to an imbalance between the red-shifted and blue-shifted power as a function of viewing direction, but it is not currently possible to extract a rotation speed from these data.
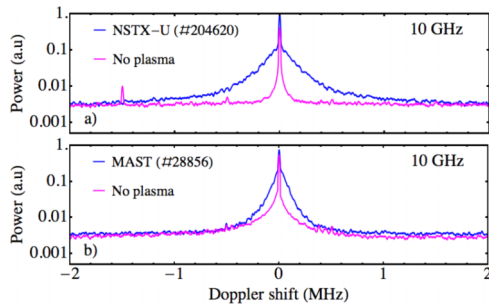
FIG. 6. Plot of the active probing spectrum on both MAST and NSTX-U shown with no plasma (magenta) and during a discharge (blue) for SAMI's lowest frequency channel (10 GHz). The increase in signal is greater in NSTX-U than in MAST due to SAMI's antenna array being closer to the plasma surface in NSTX-U.
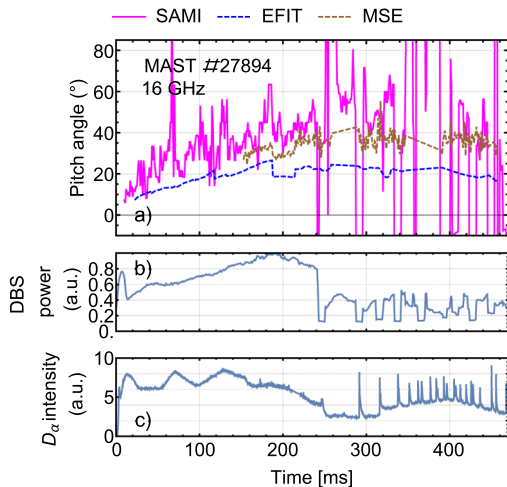

FIG. 7. Data from MAST shot 27894 operating in L-mode before 240 ms and H-mode thereafter. Panel (a) compares the SAMI measurement (magenta) of the edge pitch angle at 16 GHz with MSE (brown) and EFIT (blue). The other panels provide contextual information for this shot.

Figure 7 shows data from MAST shot 27894 and compares the SAMI magnetic pitch angle measurement (shown in magenta) with unconstrained EFIT (shown in blue) and the motional Stark effect (MSE) measurement (shown in brown). This measurement is made at 16 GHz, corresponding to a density surface that is just outside the last closed flux surface. The data from SAMI, MSE, and EFIT follow the same trend, but the SAMI-measured pitch angle is larger than the EFIT calculation (with the MSE measurement located between EFIT and SAMI). At around 240 ms, the discharge transitions from L-mode to H-mode (as can be seen in the D_α spectrum shown in panel (c)). During this later period (as shown in panel (b)), the Doppler-shifted power reduces so much that a SAMI reconstruction becomes impossible. This is due to the reduction in the amplitude of edge turbulence associated with H-mode. This problem could be overcome by increasing the power in the probing beam.

Figures 8 and 9 show data from NSTX-U shots 204620 and 204944. The SAMI magnetic pitch angle measurement (shown in magenta) is compared with unconstrained EFIT (shown in blue). (MSE data are not available for these shots.) These measurements are made at 10 GHz and 16 GHz, corresponding to a density surface outside and just inside the
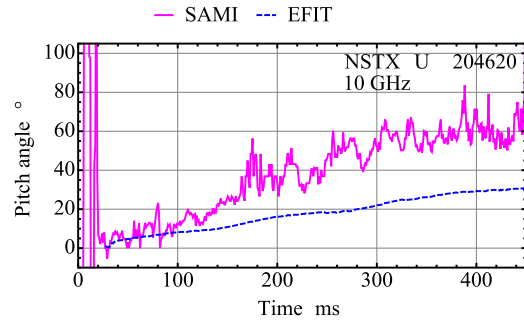

FIG. 8. SAMI measurement (magenta) of the edge pitch angle at 10 GHz of NSTX-U shot 204620 operating in L-mode before 250 ms and H-mode thereafter compared with EFIT (blue).
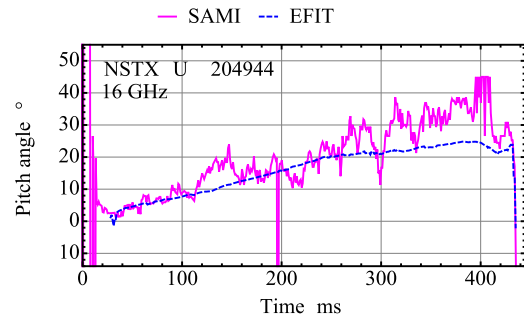

FIG. 9. SAMI measurement (magenta) of the edge pitch angle at 16 GHz of NSTX-U shot 204944 operating in L-mode compared with EFIT (blue).

last closed flux surface (LCFS), respectively. As on MAST, the SAMI measurements qualitatively follow the EFIT estimates but are larger. In shot 204620 (Fig. 8) the plasma enters H-mode at approximately 250 ms. At this time, the SAMI Doppler-shifted power experiences a reduction, but not to the same extent as seen on MAST, thereby enabling SAMI to continue working. We note that the agreement with EFIT is much better for shot 204944 than 204620. Without a larger dataset, it is not possible to say whether this discrepancy in level of agreement is a physics result (e.g., associated with moving inside the LCFS) or coincidence.

VII. SUMMARY AND FUTURE WORK

In this paper, we have motivated SAMI in terms of needing a direct measurement of the edge current density in order to develop and constrain models for ELMs. Having briefly described the principles of phased-array imaging and the SAMI hardware, we presented new results comparing the edge pitch angle measured by SAMI with EFIT and MSE on MAST, and with EFIT on NSTX-U. The SAMI measurements agree qualitatively with EFIT on both MAST and NSTX-U but are typically larger throughout the measurement window; this discrepancy is currently unexplained. It is perhaps interesting that the MSE measurement on MAST, which is less well-resolved spatially than SAMI, also over-estimates the pitch angle compared to EFIT. In summary we claim that SAMI has demonstrated the feasibility of measuring the edge pitch angle via 2-D Doppler back-scattering.

Moving the SAMI methodology from proof-of-principle to production quality requires a number of technical upgrades that we look forward to implementing in the near future: (a) an

increase in the number of antennas to reduce the side-lobe power; (b) the separation of polarisations to reduce interference between O-mode and X-mode reflections; and (c) acquisition of two frequencies simultaneously so that time-resolved measurements of the magnetic shear (and thence current density) can be obtained.

ACKNOWLEDGMENTS

[1]H. Zohm, Plasma Phys. Controlled Fusion **38**, 105 (1996).

[2]R. Scannell, M. Walsh, M. Dunstan, J. Figueiredo, G. Naylor, T. O'Gorman, S. Shibaev, K. Gibson, and H. Wilson, Rev. Sci. Instrum. **81**, 10D520 (2010).

[3]B. LeBlanc, A. Diallo, G. Labik, and D. Stevens, Rev. Sci. Instrum. **83**, 10D527 (2012).

[4]B. S. Victor, C. T. Holcomb, S. L. Allen, W. H. Meyer, M. A. Makowski, and A. Thorman, Rev. Sci. Instrum. **87**, 11E126 (2016).

[5]E. Viezzer, R. Dux, M. G. Dunne, and ASDEX Upgrade Team, Rev. Sci. Instrum. **87**, 11E528 (2016).

[6]O. Meneghini and F. A. Volpe, Rev. Sci. Instrum. **87**, 11E120 (2016).

[7]M. Ryle and A. Hewish, Mon. Not. R. Astron. Soc. **120**, 220 (1960).

[8]M. Ryle, Nature **239**, 435 (1972).

[9]A. Thompson, J. Moran, and G. Swenson, Jr., *Interferometry and Synthesis in Radio Astronomy* (John Wiley & Sons, 2008).

[10]E. Holzhauer, M. Hirsch, T. Grossmann, B. Brañas, and F. Serra, Plasma Phys. Controlled Fusion **40**, 1869 (1998).

[11]D. Thomas, K. Brunner, S. Freethy, B. Huang, V. Shevchenko, and R. Vann, Nucl. Fusion **56**, 026013 (2016).

[12]V. F. Shevchenko, R. G. Vann, S. J. Freethy, and B. K. Huang, J. Instrum. **7**, P10016 (2012).

[13]S. Freethy, V. Shevchenko, and R. Vann, IEEE Trans. Antennas Propag. **60**, 5442 (2012).

[14]B. Huang *et al.*, Fusion Eng. Des. **87**, 2106 (2012).

[15]K. Brunner, J. Chorley, N. Dipper, G. Naylor, R. Sharples, G. Taylor, D. Thomas, and R. Vann, Rev. Sci. Instrum. **87**, 11E129 (2016).

[16]J. Chorley, R. Akers, K. Brunner, N. Dipper, S. J. Freethy, R. Sharples, V. Shevchenko, D. A. Thomas, and R. G. Vann, Fusion Sci. Technol. **69**, 643 (2016).

[17]I. Chapman *et al.*, Nucl. Fusion **55**, 104008 (2015).

[18]S. Freethy, B. Huang, V. Shevchenko, and R. Vann, Plasma Phys. Controlled Fusion **55**, 124010 (2013).

[19]S. Freethy, K. McClements, S. C. Chapman, R. Dendy, W. Lai, S. Pamela, V. F. Shevchenko, and R. Vann, Phys. Rev. Lett. **114**, 125004 (2015).

[20]J. Menard *et al.*, Nucl. Fusion **52**, 083015 (2012).